AIAA JOURNAL
Vol. 50, No. 6, June 2012

Computational Investigation into the Use of Response Functions for Aerodynamic-Load Modeling

Mehdi Ghoreyshi,* Adam Jirásek,* and Russell M. Cummings†
U.S. Air Force Academy, USAFA, Colorado 80840

DOI: 10.2514/1.J051428

The generation of reduced-order models for the evaluation of unsteady and nonlinear aerodynamic loads are investigated. The reduced-order model considered is an indicial theory based on the convolution of step functions with the derivative of the input signal. The step functions are directly calculated using the results of unsteady Reynolds-averaged Navier–Stokes simulations and a grid-movement tool. Results are reported for a two-dimensional airfoil and an unmanned combat air vehicle configuration. Wind-tunnel data are first used to validate the prediction of static and unsteady coefficients at both low and high angles of attack, with good agreement obtained for all cases. The generation of the aerodynamic models is then described. The focus of the paper next shifts to assess the validity of studied reduced-order models with respect to new maneuvers. This is accomplished by comparison of the model output with time-accurate computational fluid dynamics simulations. Results presented demonstrate the feasibility of the approach for modeling unsteady aerodynamic loads and response-type computational fluid dynamics calculations.

Nomenclature

a	=	acoustic speed, m/s
$a(t)$	=	step response function
C_L	=	lift coefficient, $L/q_\infty S$
C_{Lq}	=	indicial lift coefficient with normalized pitch rate, 1/rad
$C_{L\alpha}$	=	indicial lift coefficient with angle of attack, 1/rad
C_{L0}	=	zero-angle-of-attack lift coefficient
C_m	=	pitching-moment coefficient, $m/q_\infty Sc$
C_{mq}	=	indicial pitching-moment coefficient with normalized pitch rate, 1/rad
$C_{m\alpha}$	=	indicial pitching-moment coefficient with angle of attack, 1/rad
C_{m0}	=	zero angle of pitching-moment coefficient
C_z	=	z-axis force coefficient, $F_z/q_\infty S$
c	=	chord, m
$f(t)$	=	forcing function
G	=	transfer function
$g(t)$	=	impulse response function
g_i	=	Volterra kernels
H	=	step function
k	=	reduced frequency, $\omega c/2V$
L	=	lift force, N
M	=	Mach number, V/a
m	=	pitching moment, N-m
p	=	pressure, Pa
$\dot{q}$	=	time rate of pitch rate, rad/s^2
$\bar{q}$	=	pitch rate, rad/s
q	=	normalized pitch rate, $\bar{q}c/V$, rad
q_∞	=	dynamic pressure, Pa
Re	=	Reynolds number, $\rho Vc/\mu$
S	=	reference area, m^2
s	=	normalized time, $2Vt/c$
t	=	time, s
t^*	=	nondimensional time step, Vt/c
t_0	=	start time, s
u, v, w	=	velocity components in X, Y and Z axis, m/s
V	=	freestream velocity, m/s
X, Y, Z	=	coordinates of a right-handed orthogonal axis
x/c	=	distance normalized by chord length
α	=	angle of attack, rad
$\dot{\alpha}$	=	normalized time rate of angle of attack, 1/rad
α_A	=	pitch amplitude, rad
α_0	=	mean angle of attack, rad
μ	=	air viscosity
ρ	=	density, kg/m^3
ω	=	circular frequency, rad/s

Presented at the 29th AIAA Applied Aerodynamic Conference, Honolulu, HI, 27–30 June 2011; received 6 June 2011; revision received 21 November 2011; accepted for publication 17 December 2011.

*NRC Research Fellow, Modeling and Simulation Research Center. Senior Member AIAA.
†Professor, Department of Aeronautics. Associate Fellow AIAA.

I. Introduction

TRADITIONALLY, the prediction of aerodynamic characteristics of an airplane during the conceptual design stage relies on handbook methods or linear fluid mechanics assumptions [1–3]. These methods provide low-cost reliable data only for conventional aircraft in aerodynamically benign regions of the flight envelope. However, current trends in aircraft design toward novel shapes, augmented stability, and expanded flight envelopes require a more accurate description of the nonlinear and unsteady aerodynamics [4]. Typical conceptual design aerodynamic prediction methods do not work well for these situations. To meet these challenging demands, a number of problems need to be resolved, including the formulation of unsteady aerodynamics loads, system identification, and use of the aerodynamic models in various design disciplines such as control model synthesis, aircraft optimization, and stability predictions. The reliable prediction of unsteady aerodynamic loads, along with system identification, is presented in this paper.

It is well known that the unsteady aerodynamic forces and moments not only depend on the instantaneous states, but also their time histories [5,6]. In particular, flow hysteresis could lead to pronounced lags in the increase and decline of aerodynamic loads with time. Abramov et al. [7] note that the normalized time lags in aerodynamic loads from vortex breakdown phenomena can be up to 15 times larger than the convective time scale. Since a full-order model of the unsteady flow around aircraft is computationally very expensive, the efforts over the last years have been spent mainly on the development of a reduced-order model (ROM) using system identification from experimental and, more recently, from numerical data [8,9].

There are only limited experimental measurements available to determine the effects of unsteady flow on the aerodynamic forces and moments acting on an aircraft. This is mainly due to the complexity of unsteady flow and the limitations of existing test facilities [10]. An alternative is to use simulations based on computational fluid dynamics (CFD). Although it is possible to study the flow around a maneuvering aircraft directly using the coupled aircraft equations of motion with the unsteady Reynolds-averaged Navier–Stokes (URANS) equations, such an approach is impractical to use for aircraft flight dynamics, due to excessive computational cost. To make progress in routinely using of CFD in aircraft design, methods based on sampling, model updating and system identification are available. Ghoreyshi et al. [11] described the sampling and reconstruction of lookup tables based on kriging interpolation models and data fusion using cokriging. The flight dynamics results of different configurations were reported using CFD-based lookup table, which can be generated at an acceptable cost [12–14]. The benefits of such lookup tables are that the tables 1) can directly be implemented into the aircraft equations of motion using interpolation schemes and 2) are consistent with the nonlinear and quasi-steady aerodynamics. However, such an approach lacks the time hysteresis arising from unsteady vortical flows. Ghoreyshi et al. [13] showed that for a fast-maneuvering aircraft with vortical flow at high angles of attack, there is a lag time between lookup table predictions and the time-marching solution. This lag emphasizes the need to investigate and develop ROMs to predict the unsteady aerodynamics at such conditions.

The aerodynamics modeling can be classified into nonparametric and parametric models [15]. The parametric models provide a structure for representing aerodynamic forces and moments in the aircraft equations of motion. The nonparametric models, on other hand, are concerned with the measured input/output behavior of the aircraft dynamics [15]. Recent efforts on the development of nonparametric models can be classified into two types: time-domain or frequency-domain approaches [16]. The frequency-domain models are obtained from matching transfer functions computed from the measured input/output data [17]. Examples of the frequency-domain ROMs are the indicial response method by Ballhaus and Goorjian [18] and Tobak et al. [19,20] and a frequency-domain model based on proper orthogonal decomposition by Hall et al. [21]. The time-domain models are based on the state-space representation by matching time histories of measured data. Some examples of time-domain ROMs include the unit sample response by Gaitonde and Jones [22], Volterra theory by Silva and Bartels [23], radial basis functions [24], and state-space modeling [25]. Current interest at the U.S. Air Force Academy (USAFA) is toward development of ROMs based on the time histories of CFD simulations of maneuvering aircraft [26–28] and design of optimal CFD-based training maneuvers for system identification [24].

The current paper aims to develop methodologies based on Volterra theory and indicial response models. Although these methods provide a fundamental approach to modeling the unsteady aerodynamics, some problems need to be addressed, such as these models change the aircraft differential equations of motion to an integro-differential type and accurate responses can only be determined analytically. The investigation of the first problem is beyond the scope of this paper. The analytical solutions are limited only to two-dimensional airfoils in incompressible and inviscid flows [29]. Besides, experimental tests are practically nonexistent for impulse and step response functions. A solution is the approximation of response functions using CFD calculations that provide quite accurate results in the absence of experimental and analytical data for a given aircraft configuration. Thus, the first objective of this work is to develop the aerodynamic load responses with the direct use of CFD computations. The application of CFD for the response function approximation raises two more questions: Are the CFD-based data valid and how to uncouple the effects of angle of attack and pitch rate from the computations of a rotating grid. For the validation aspect, the CFD prediction will be validated against available static and dynamic wind-tunnel data. With respect to uncoupling the effects of angle of attack and the pitch rate, a new approach using grid motion tool will be implemented. Finally, the accuracy of the aerodynamic models will be compared with time-dependent CFD computations of new maneuvers.

II. Response-Driven ROMs

ROMs represent the solution of the output signal $y(t)$ for any arbitrary forcing function (or boundary condition) $f(t)$, without the need for the full system simulation. A way to represent the boundary-output relationship is to find the response of the output signal to an impulse, $\delta(t)$, or a unit step, $H(t)$, change of the boundary condition that are defined as

$$\delta(t) = \begin{cases} 1.0 & \text{for } t = 0 \\ 0.0 & \text{for } t \neq 0 \end{cases} \tag{1}$$

$$H(t) = \begin{cases} 1.0 & \text{for } t \geq 0 \\ 0.0 & \text{for } t < 0 \end{cases} \tag{2}$$

The impulse response and unit response are denoted by $g(t)$ and $a(t)$, respectively, (the unit response is also called the indicial admittance). An example of an impulse-type ROM is the Volterra theory that is considered as one of the most important tools for the representation of nonlinear systems where the system output depends on the current and past values of the input. Such a system is called a dynamic system (i.e., a system with memory) [30]. The approach was first introduced by Vito Volterra in a book published in 1930 [31]. This work and the further developments by others (for example, Wiener [32], Barrett [33], and Kalman [34]) have been extensively used in electrical and biological systems engineering [35–39]. Recently, there is an increasing interest in using Volterra series in the field of aerodynamic loads modeling [26,40].

Assume that the system output function y at some fixed instant t_0 is the nonlinear functional of values of the forcing function f over some finite interval, for example, $a \leq t \leq b$. The output and input relationship can be expressed as

$$y(t_0) = F(f(t), a \leq t \leq b) \tag{3}$$

Volterra expanded Eq. (3) as a power series:

$$\bar{y}(t_0) = \sum_{n=0}^{\infty} F_n[f(t)] \tag{4}$$

where F_0 (named the zeroth-order Volterra function) is a constant ($F_0 = g_0$). For any $n \geq 1$, F_n shows the nth order Volterra functional [31] and is a n-dimensional convolution of the function $f(t)$ and function $g_n(\tau_1, \tau_2, \ldots, \tau_n)$. The functions $g_0, g_1, \ldots g_n$ are called Volterra kernels and related to the impulse functions of the system [41,42]. For the values of y at any time $t \geq 0$, the Volterra expansion is expressed as

$$\begin{aligned} \bar{y}(t) = {} & g_0 + \int_0^t g_1(t-\tau_1) f(\tau_1)\, \mathrm{d}\tau_1 \\ & + \int_0^t \int_0^t g_2(t-\tau_1, t-\tau_2) f(\tau_1) f(\tau_2)\, \mathrm{d}\tau_1\, \mathrm{d}\tau_2 + \cdots \\ & + \int_0^t \int_0^t \cdots \int_0^t g_n(t-\tau_1, t-\tau_2, \ldots, \\ & \quad t-\tau_n) f(\tau_1) f(\tau_2) \cdots f(\tau_n)\, \mathrm{d}\tau_1\, \mathrm{d}\tau_2 \cdots \mathrm{d}\tau_n \end{aligned} \tag{5}$$

Although this model can approximate any finite-memory, time-invariant, single-input/single-output, and continuous nonlinear system [30], the computational determination of system impulse response may be complicated, as it occurs over a very short period of time [43]. Thus, it is more common to use indicial response.

Assuming a linear relationship between the forcing function and the output, a ROM is defined as the convolution (or Duhamel's superposition [44]) of the indicial response with the derivative of the forcing function [45]:

$$\bar{y}(t) = \frac{\mathrm{d}}{\mathrm{d}t}\left[\int_0^t a(t-\tau)f(\tau)\,\mathrm{d}\tau\right] \tag{6}$$

Note that a linear Volterra system and the linear step-type ROM given in Eq. (6) are identical. For a linear system, g_1 is the impulse response function and $g_1(t) = \mathrm{d}a(t)/\mathrm{d}t$ applies. The indicial response functions are used as a fundamental approach to represent the unsteady aerodynamic loads. The mathematical models are detailed by Tobak et al. [19,20] and Reisenthel et al. [46,47]. The longitudinal aerodynamic forces and moments are considered in this paper. We denote the time responses in lift due to the step changes in angle of attack α and angular velocity q as $C_{L\alpha}$ and C_{Lq}, respectively. If these functions are known, then the total lift coefficient at time t can be obtained using Eq. (7):

$$C_L(t) = C_{L0} + \frac{\mathrm{d}}{\mathrm{d}t}\left[\int_0^t C_{L\alpha}(t-\tau)\alpha(\tau)\,\mathrm{d}\tau\right] + \frac{\mathrm{d}}{\mathrm{d}t}\left[\int_0^t C_{Lq}(t-\tau)q(\tau)\,\mathrm{d}\tau\right] \tag{7}$$

where C_{L0} denote the zero-angle-of-attack lift coefficient. Similarly, the pitching moment is estimated as follows:

$$C_m(t) = C_{m0} + \frac{\mathrm{d}}{\mathrm{d}t}\left[\int_0^t C_{m\alpha}(t-\tau)\alpha(\tau)\,\mathrm{d}\tau\right] + \frac{\mathrm{d}}{\mathrm{d}t}\left[\int_0^t C_{mq}(t-\tau)q(\tau)\,\mathrm{d}\tau\right] \tag{8}$$

where C_{m0} shows the zero-angle-of-attack pitching-moment coefficient. For nonlinear aerodynamics, the dependency on the angle of attack are added to the indicial functions: i.e.,

$$C_L(t) = C_{L0} + \frac{\mathrm{d}}{\mathrm{d}t}\left[\int_0^t C_{L\alpha}(t-\tau,\alpha)\alpha(\tau)\,\mathrm{d}\tau\right] + \frac{\mathrm{d}}{\mathrm{d}t}\left[\int_0^t C_{Lq}(t-\tau,\alpha)q(\tau)\,\mathrm{d}\tau\right] \tag{9}$$

$$C_m(t) = C_{m0} + \frac{\mathrm{d}}{\mathrm{d}t}\left[\int_0^t C_{m\alpha}(t-\tau,\alpha)\alpha(\tau)\,\mathrm{d}\tau\right] + \frac{\mathrm{d}}{\mathrm{d}t}\left[\int_0^t C_{mq}(t-\tau,\alpha)q(\tau)\,\mathrm{d}\tau\right] \tag{10}$$

It is deemed wise to evaluate the response functions at intervals rather than each angle of attack. For example, to determine $C_{L\alpha}(t,\alpha)$ and $C_{m\alpha}(t,\alpha)$ terms, one might find the responses to the lower and upper angles of the interval. The difference between these responses divided by the interval length results in the indicial functions at the interval. A linear interpolation scheme is then used to find the functions at different angles of attack.

III. Determination of Step Responses

For compressible and three-dimensional cases, the only direct method for determination of the impulse and unit response functions is CFD. Raveh [48], for example, studied the use of CFD for development of ROMs based on the impulse and unit step functions. Raveh showed that the accuracy of ROM based on the impulse response is highly sensitive to the choice of forcing function amplitude and computational time step, while the CFD-based response to the unit step function was proven to be more robust and practical to use.

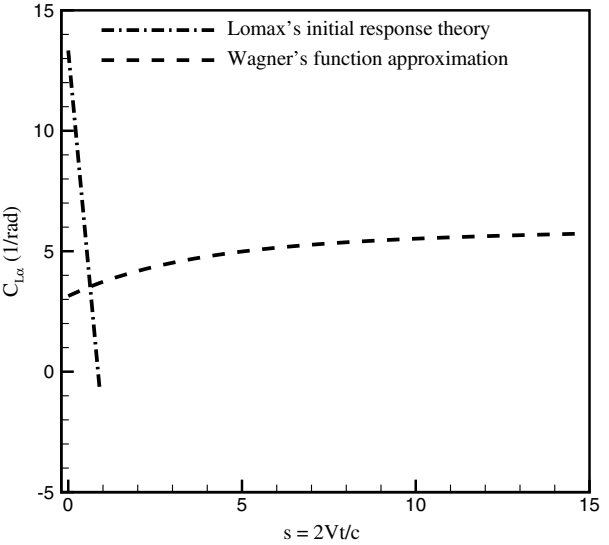

Fig. 1 Lomax's and Wagner's values at $M = 0.3$.

The values of initial and final points of the indicial response function are well established for the two-dimensional case. Lomax [49] used the linearized Euler equations to derive exact initial values of the compressible indicial response of a flat plate airfoil to a step change in angle of attack, and his equation was expressed as

$$C_{L\alpha} = \frac{4}{M}\left(1 - \frac{1-M}{2M}s\right) \tag{11}$$

where M is the Mach number and $s = 2Vt/c$ is the normalized time. Wagner [50] also studied the lift response of incompressible flow a short time after a step change in angle of attack is applied. His function was approximated in nondimensional time by a two-pole exponential function as [51]:

$$C_{L\alpha} = 2\pi(1 - 0.165e^{-0.0455s} - 0.33e^{-0.3s}) \tag{12}$$

These analytical functions are shown graphically in Fig. 1 for $M = 0.3$. Bisplinghoff et al. [52] described an exponential approximation to the exact solutions of $C_{L\alpha}$ and $C_{m\alpha}$ for various Mach numbers. Again, for airfoils, Mazelsky [53] and Leishman [44] reported the initial and final values of the indicial lift due to a step change in the pitch rate as

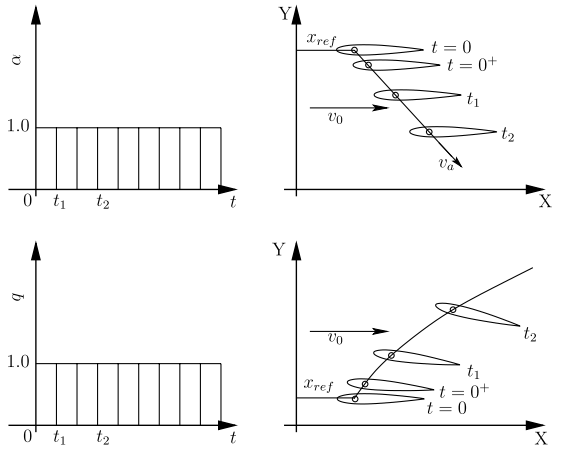

Fig. 2 Grid motion for modeling a step change in angle of attack and pitch rate.

$$C_{Lq}(s=0) = [2(1-2\bar{x}_a)/M] \tag{13}$$

$$C_{Lq}(s\to\infty) = (\pi/\sqrt{1-M^2})[(3-4\bar{x}_a)/2] \tag{14}$$

where $\bar{x}_a$ shows the pitch-axis location. For three-dimensional configurations, Queijo et al. [54] also detailed some approximate functions for the indicial lift function of tapered, swept wings in incompressible flow. However, there is no indicial function available for three-dimensional aircraft with compressible flow. In fact, the step function is a mathematical concept and the exact solution probably cannot be determined by direct experiments [55]. There are only a few published solutions for the indicial response using CFD for airfoils and wings only (see, for example, Manglano-Villamarin and Shaw [56], Singh and Baeder [29], and Raveh [48]). The present paper describes a method of calculating indicial functions using CFD. The methodology and solver used are described below.

Table 1 Description of the AGARD CT2 test conditions

Test conditions	Values
Mach number M_∞	0.6
Mean incidence α_0	3.16 deg
Pitch amplitude α_A	4.59 deg
Reduced frequency k	0.0811
Reynolds number Re	4.8×10^6

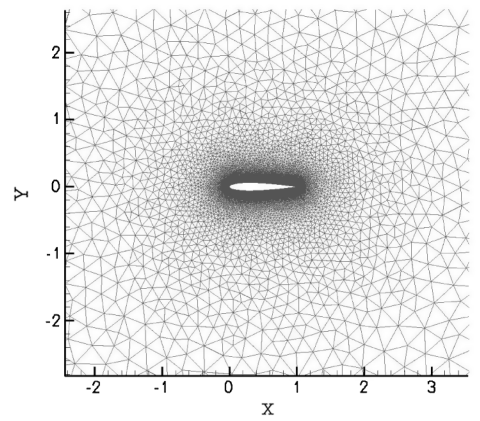

a) NACA0012 global grid view

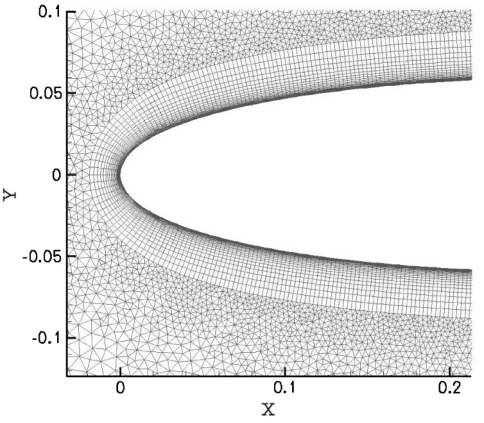

b) NACA0012 viscous layer

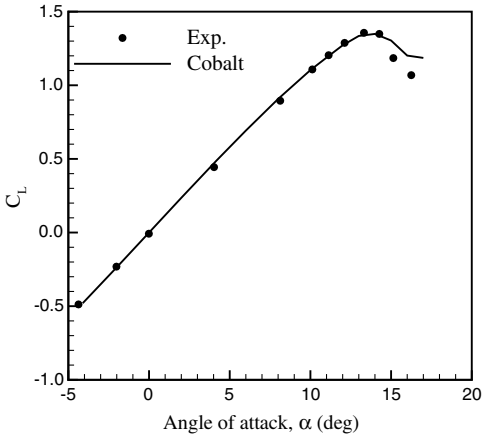

c) Static lift coefficient

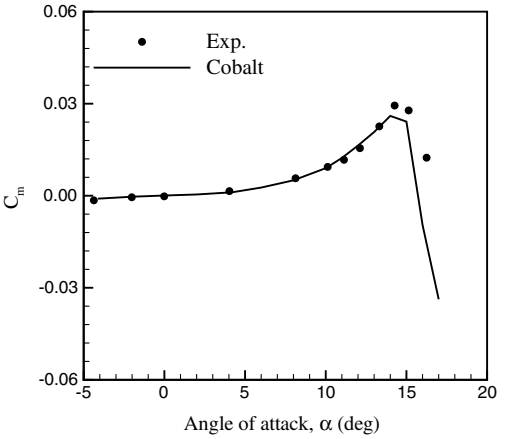

d) Static pitching moment coefficient

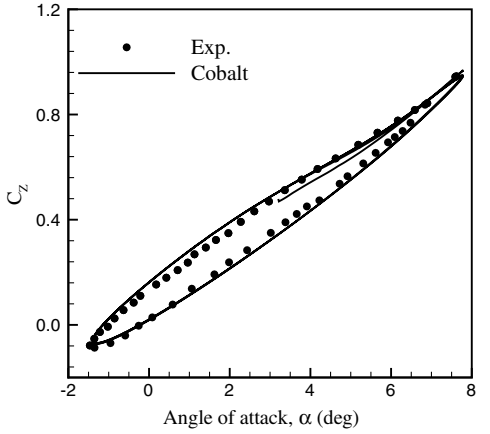

e) Z-force coefficient of AGARD CT2

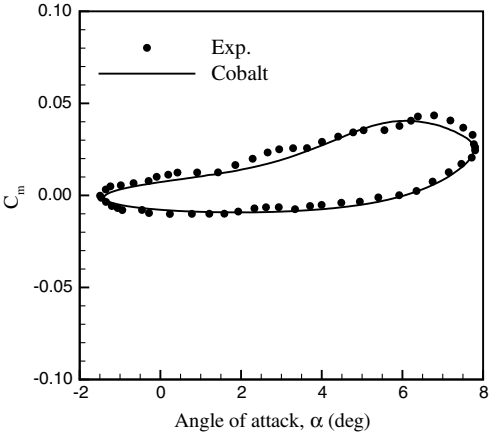

f) Pitching moment coefficient of AGARD CT2

Fig. 3 NACA 0012 grid and static and dynamic validations. The static conditions are : $M_\infty = 0.3$ and $Re = 5.93 \times 10^6$. Static and AGARD CT2 experimental data are from Ladson [65] and Landon [66], respectively.

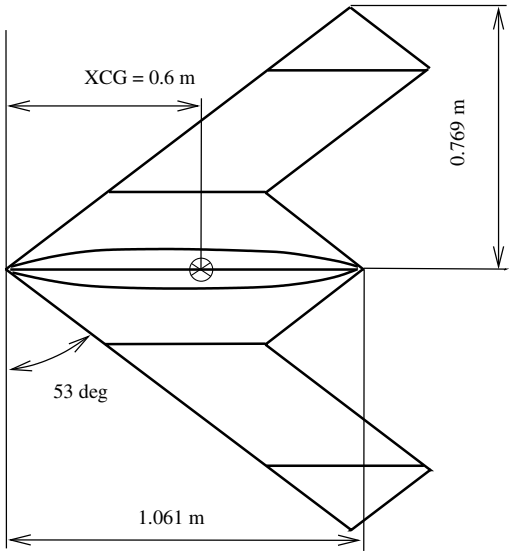

Fig. 4 SACCON geometry [68].

IV. CFD Formulation

A. CFD Solver

The flow solver used for this study is the commercially available flow solver Cobalt [57] that solves the unsteady, three-dimensional, and compressible Navier–Stokes equations. The Navier–Stokes equations are discretised on arbitrary grid topologies using a cell-centered finite volume method. Second-order accuracy in space is achieved using the exact Riemann solver of Gottlieb and Groth [58] and least-squares gradient calculations using *QR* factorization. To accelerate the solution of discretized system, a point-implicit method using analytic first-order inviscid and viscous Jacobian is used. A Newtonian subiteration method is used to improve time accuracy of the point-implicit method. The method is second-order-accurate in time. Tomaro et al. [59] converted the code from explicit to implicit, enabling Courant–Friedrichs–Lewy numbers as high as 10^6. The Cobalt solver has been used at the U.S. Air Force Seek Eagle Office and USAFA for a variety of unsteady nonlinear aerodynamic problems of maneuvering aircraft [60–64].

B. Motion Simulations

Cobalt uses an arbitrary Lagrangian–Eulerian formulation and hence allows all translational and rotational degrees of freedom [28]. For the control-surface simulations, an overset-grid capability is available. The code can simulate both free and specified six-degree-of-freedom (6-DOF) motions. The rigid motion is specified from a motion input file. For the rigid motion the location of a reference

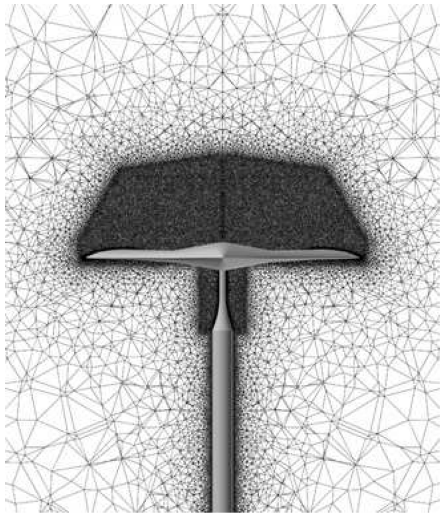

a) SACCON grid

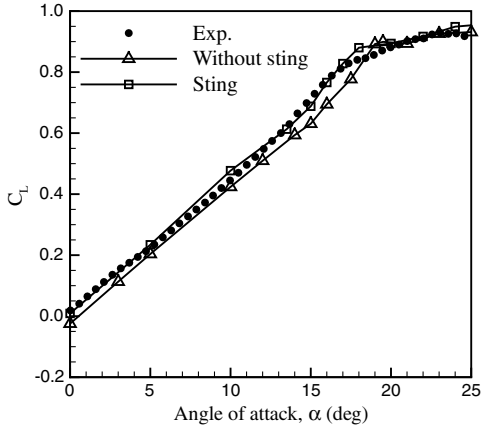

b) Static lift coefficient

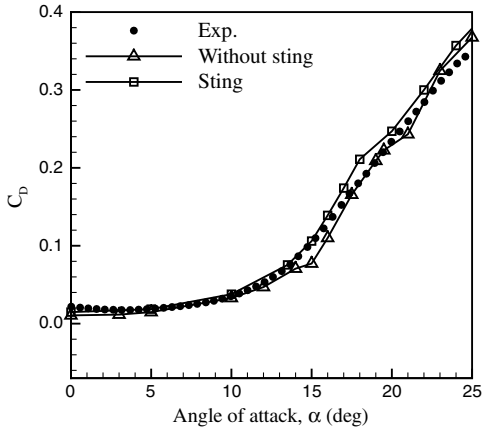

c) Static drag coefficient

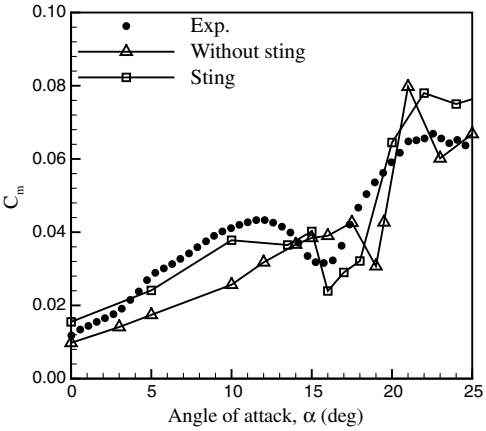

d) Static pitching moment coefficient

Fig. 5 SACCON grid and static validations. The static conditions are : $M_\infty = 0.144$ and $Re = 1.61 \times 10^6$. Experiments are obtained from Cummings and Schütte [68] and shown with filled circles. The solid lines with delta markers show the Cobalt predictions for a grid without sting geometry. The lines with square marker shows predictions of a grid including sting geometry. Turbulence model is SARC.

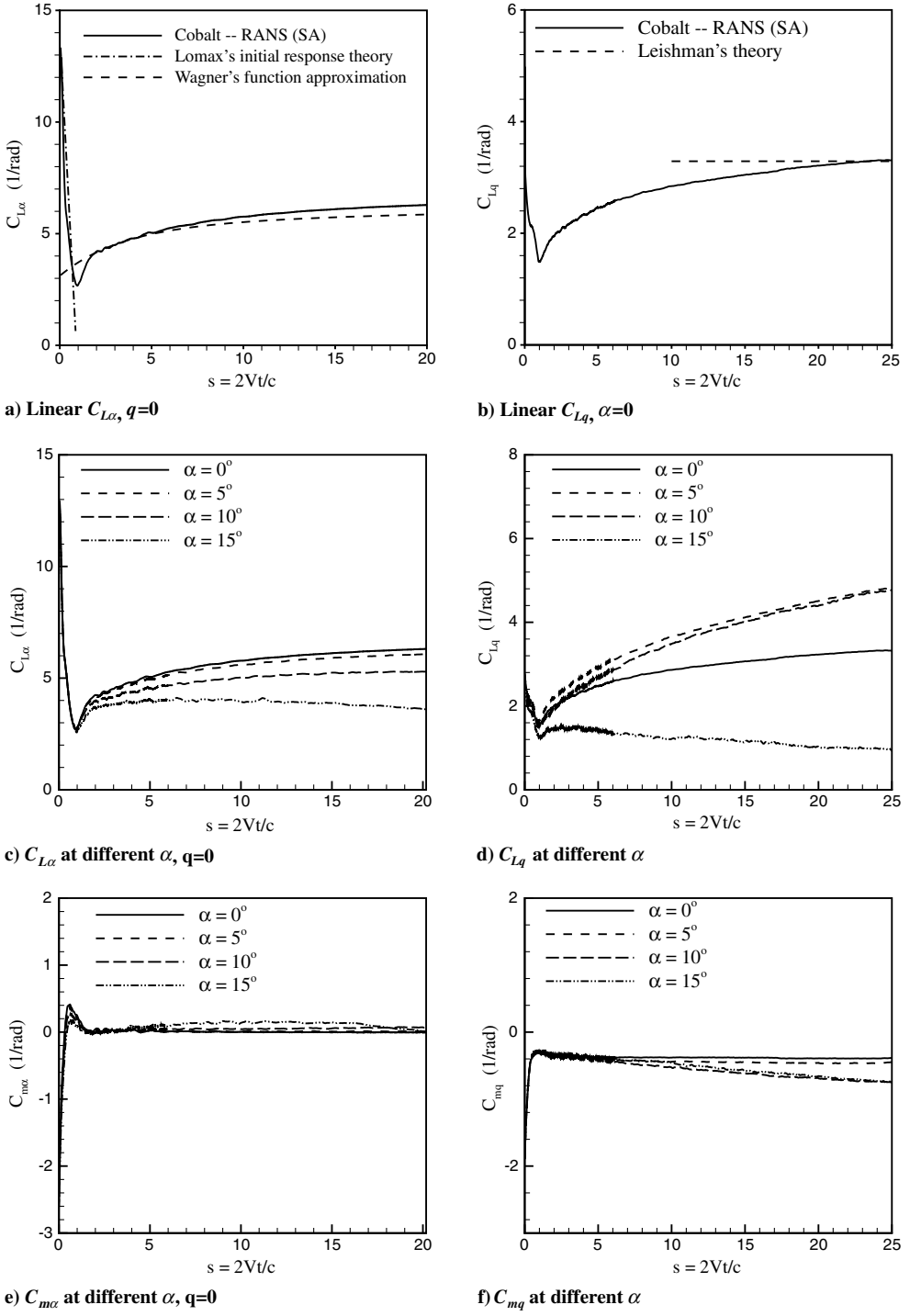

a) Linear $C_{L\alpha}$, q=0 **b) Linear C_{Lq}, α=0**

c) $C_{L\alpha}$ at different α, q=0 **d) C_{Lq} at different α**

e) $C_{m\alpha}$ at different α, q=0 **f) C_{mq} at different α**

Fig. 6 NACA 0012 lift and pitching-moment indicial functions at $M_\infty = 0.3$ and $Re = 5.93 \times 10^6$.

point on the aircraft is specified at each time step. In addition the rotation of the aircraft about this reference point is also defined using the rotation angles of yaw, pitch, and bank. The aircraft reference-point velocity v_a in an inertial frame is then calculated to achieve the required angles of attack and side slip, as well as the forward speed. The velocity is then used to calculate the location. The initial aircraft velocity v_0 is specified in terms of Mach number, angle of attack, and sideslip angle in the main file. The instantaneous aircraft location for the motion file is then defined from the relative velocity vector, $v_a - v_0$.

The grid motion is used to calculate the indicial response. This approach allows the uncoupling of effects of angle of attack and pitch rate for the indicial functions. As an example for a step change in angle of attack, the grid immediately starts to move at $t = 0$ to the right and downward, as shown in Fig. 2. The translation continues over time with a constant-velocity vector. Since there is no rotation, all the effects in aerodynamic loads are from changes in the angle of attack. For a unit step change in pitch rate, the grid moves and rotates simultaneously. The grid starts to rotate with a unit pitch rate at $t = 0$. To hold the angle of attack zero during the rotation, the grid moves right and upward in Fig. 2.

V. Test Cases and Validation

A two-dimensional airfoil and a generic unmanned combat air vehicle (UCAV) stability and control configuration (SACCON) are considered in this paper. More details on these cases are provided below.

A. Two-Dimensional Airfoil

The steady and unsteady simulations of the NACA 0012 airfoil using Cobalt are considered. The computational domain is rectangular with the airfoil geometry centrally located. The minimal distance from the body to each of the outer boundaries is $20c$, where c is the airfoil chord, which is 1 m. No-slip, adiabatic-wall boundary conditions are employed at the body surface, and modified Riemann-invariant conditions were implemented at the far-field boundary. The mesh consists of prisms and tetrahedra and was generated using SolidMesh 2D. Jirásek et al. [24] performed the sensitivity study of the grid size and time step. The pitch axis and the moment reference point are set to $0.25c$ for all the results. The overview of the fine mesh is shown in Figs. 3a and 3b.

Experimental data for the steady and unsteady aerodynamics of the NACA 0012 airfoil are available (see, for example, Ladson [65] and Landon [66]). For steady simulations, the flow conditions correspond to $M_\infty = 0.3$ and $Re = 8.93 \times 10^6$. All simulation were performed using the Spalart–Allmaras (SA) turbulence model. The predictions of lift and pitching-moment coefficients are compared with experimental data [65] in Figs. 3c and 3d A very good agreement is obtained for the angles below 15 degrees. The SA model also accurately predicts the maximum lift, but the stall region predictions do not match as well, although the results are quite good.

A pitch-oscillation test case (AGARD CT2) was selected with available experimental data [66]. The AGARD CT2 test conditions are summarized in Table 1. The CFD simulation runs for three cycles with a nondimensional time step of $\Delta t^* = 0.01$. For more details of time-step selection, the reader is referred to the work of Cummings et al. [67]. The results are shown against experimental data in Fig. 3. Even for this unsteady case, very good agreement is found, although the angles of attack fall within the linear range of α. These predictions give confidence in the ability of the current numerical approach to predict unsteady aerodynamics.

B. SACCON UCAV

The SACCON geometry and experimental data were provided to the partners participating in NATO RTO Task Group AVT-161 (Assessment of Stability and Control prediction Methods for NATO Air and Sea Vehicles) [68]. The objective of this task group is to evaluate CFD codes against wind-tunnel results. The vehicle planform and section profiles were defined in cooperation between the DLR, German Aerospace Center and EADS-MAS. DLR adjusted the predesign geometry for wind-tunnel design purposes, which actually led to a higher overall thickness at the root chord to provide enough space for the internal strain gauge balance. The aircraft has a lambda wing planform with a leading-edge sweep angle of 53 deg, as shown in Fig. 4. The root chord is approximately 1 m, the wing span is 1.53 m, the reference chord is 0.48 m, and the reference area is 0.77 m^2. The main sections of the model are the fuselage, wing section, and wing tip. The configuration is defined by three different profiles at the root section of the fuselage, two sections with the same profile at the inner wing, forming the transition from the fuselage to wing and the outer wing section. Finally, the outer wing section profile is twisted by 5 deg around the leading edge to reduce the aerodynamic loads and shift the onset of flow separation to higher angles of attack.

The wind-tunnel model was designed and manufactured at NASA Langley Research Center (LaRC). The model was designed to accommodate a belly sting mount for tests in the German-Dutch Low Speed Wind Tunnel (DNW-NWB) at DLR in Braunschweig and the $14' \times 22'$ low-speed wind tunnel at NASA LaRC [68,69]. The high-angle-of-attack flow around SACCON is very complicated and

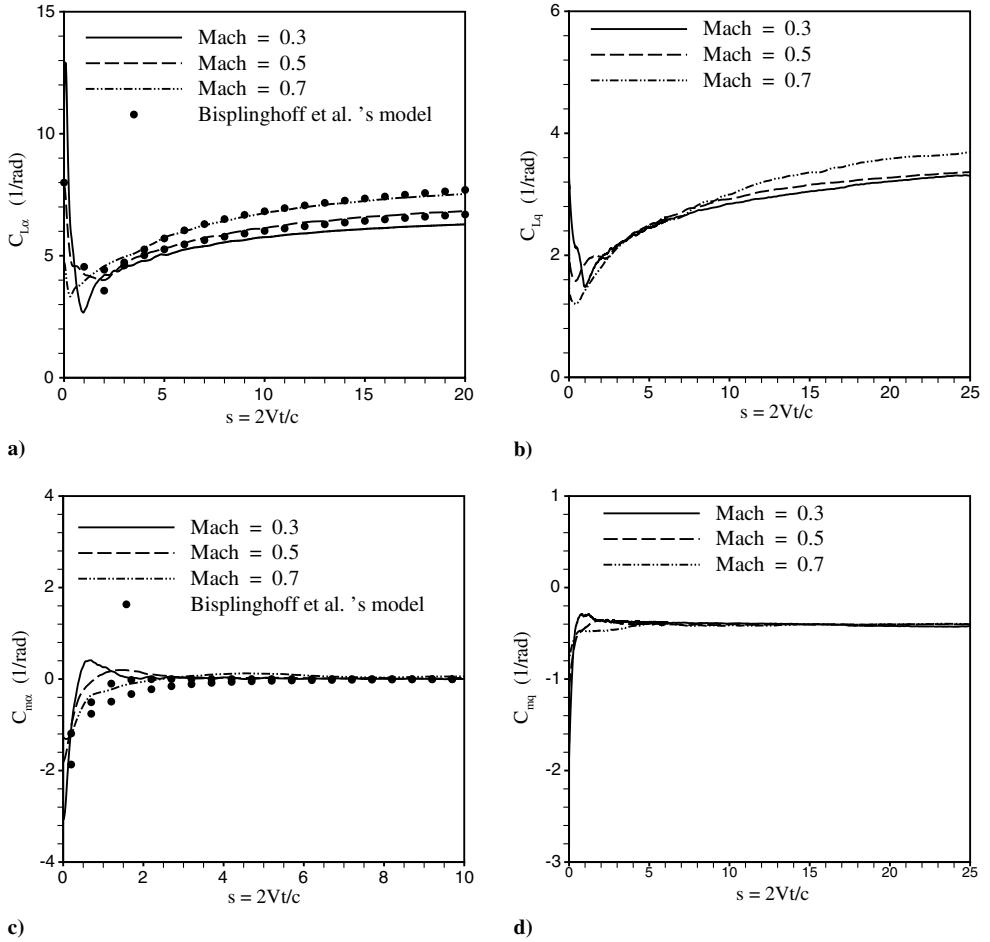

Fig. 7 Effects of Mach number on the NACA 0012 lift and pitching-moment indicial functions with unit step change of angle of attack and pitch rate. Bisplinghoff et al.'s model [52] corresponds to Mach numbers of 0.5 and 0.7.

unsteady, due to vortical flow formation, vortex interaction, and vortex breakdown [70]. Validation of CFD codes for predicting these phenomena can be a very challenging task.

Two meshes are available, the first uses a belly-mounted sting present in the experiments and the second has no sting. The meshes were generated in two steps. In the first step, the inviscid tetrahedral mesh was generated using the ICEMCFD code. This mesh was then used as a background mesh by TRITET [71,72], which builds prism layers using an advancing-front technique. TRITET rebuilds the inviscid mesh while respecting the size of the original inviscid mesh from ICEMCFD. The grid including sting geometry is shown in Fig. 5. This grid contains around 4.5 million points and 13 million cells. All CFD simulations were run on Chugach at the U.S. Department of Defense Arctic Region Supercomputing Center (ARSC) using detached-eddy simulations on the SA with rotation-correction (SARC) turbulence model. The total run time of 1000 iterations for the model without sting geometry was 5 h using 128 processors.

The coefficients of lift, drag, and pitching moment are compared with experiments in Fig. 5. The figure shows that the CFD predictions closely follow the trends of experimental data up to moderate angles of attack. The offsets in low-angle-of-attack pitching moment in the model is likely due to the effects of the belly sting mounting present in the experiments [73]. For the ROM studies, the mesh without sting geometry was used, since it has less grid points.

VI. Results and Discussion

A. NACA 0012 Airfoil

The indicial responses of the airfoil with a unit step change of angle of attack and pitch for $C_{L\alpha}$ and C_{Lq} are shown in Figs. 6a and 6b, where the indicial functions per radian are plotted against nondimensional time. The lift has a peak at $s = 0$ followed by a rapidly falling trend. The lift again builds up and asymptotically reaches the steady-state value. The initial peak can be explained based on the energy of acoustic wave systems created by the initial perturbation [44,49]. The lift magnitudes at the initial and final times of the response are favorably comparable with the analytical results of Lomax [49], Wagner [50], and Leishman [44]. The effects of angle of attack on indicial functions are shown in Figs. 6c–6f. The nonlinear response functions are calculated with the approach described earlier. Figures 6c–6f show that the initial values of indicial functions are invariant with angle of attack, but the transient trend and steady-state values change, depending on the angle of attack.

The effects of Mach number for response functions are shown in Fig. 7. The most obvious difference is that the initial peak becomes smaller for compressible flow. An explanation is given by Leishman [44]: this is due to the propagation of pressure disturbances at the speed of sound, compared with the incompressible case, where the disturbances propagate at infinite speed. Note that the initial peak values from CFD calculation at different Mach numbers closely match the analytical values from Eqs. (11) and (13).

Now a ROM was created using Eqs. (7) and (8) and used for prediction in order to check the validity of the ROMs for several motions. For a pitch oscillation with reduced frequencies of $k = 0.077$ and $k = 0.307$, with mean incidence α_0 of zero degrees and amplitude α_a of 1.0 deg, the results of the linear reduced-order model are compared with the time-marching solution in Fig. 8. The figures show that the ROM provides very good agreement for slow and fast pitching motions. The model also accurately predicts the initial peaks in full-order simulations at the beginning of the oscillations. Note that the initial responses of aerodynamic

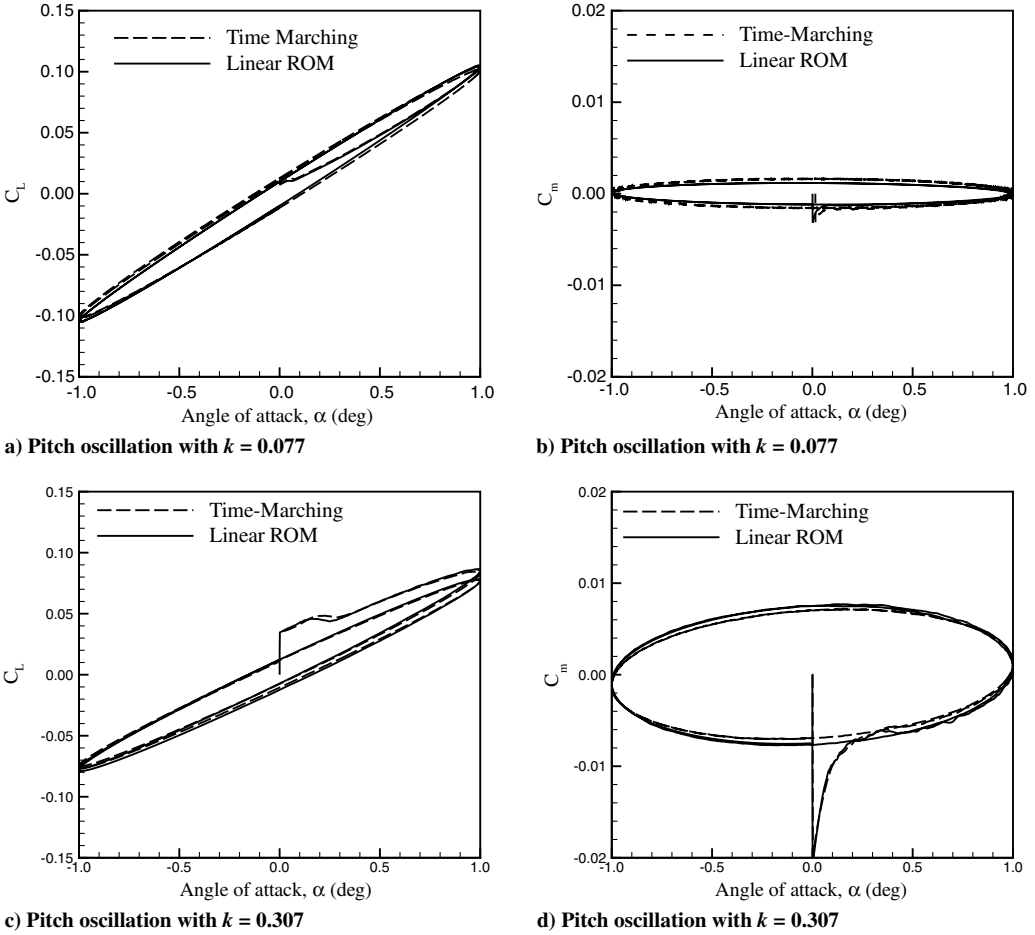

a) Pitch oscillation with $k = 0.077$ **b) Pitch oscillation with $k = 0.077$**

c) Pitch oscillation with $k = 0.307$ **d) Pitch oscillation with $k = 0.307$**

Fig. 8 Linear indicial response ROM model for the airfoil, $M_\infty = 0.3$ and $Re = 5.93 \times 10^6$.

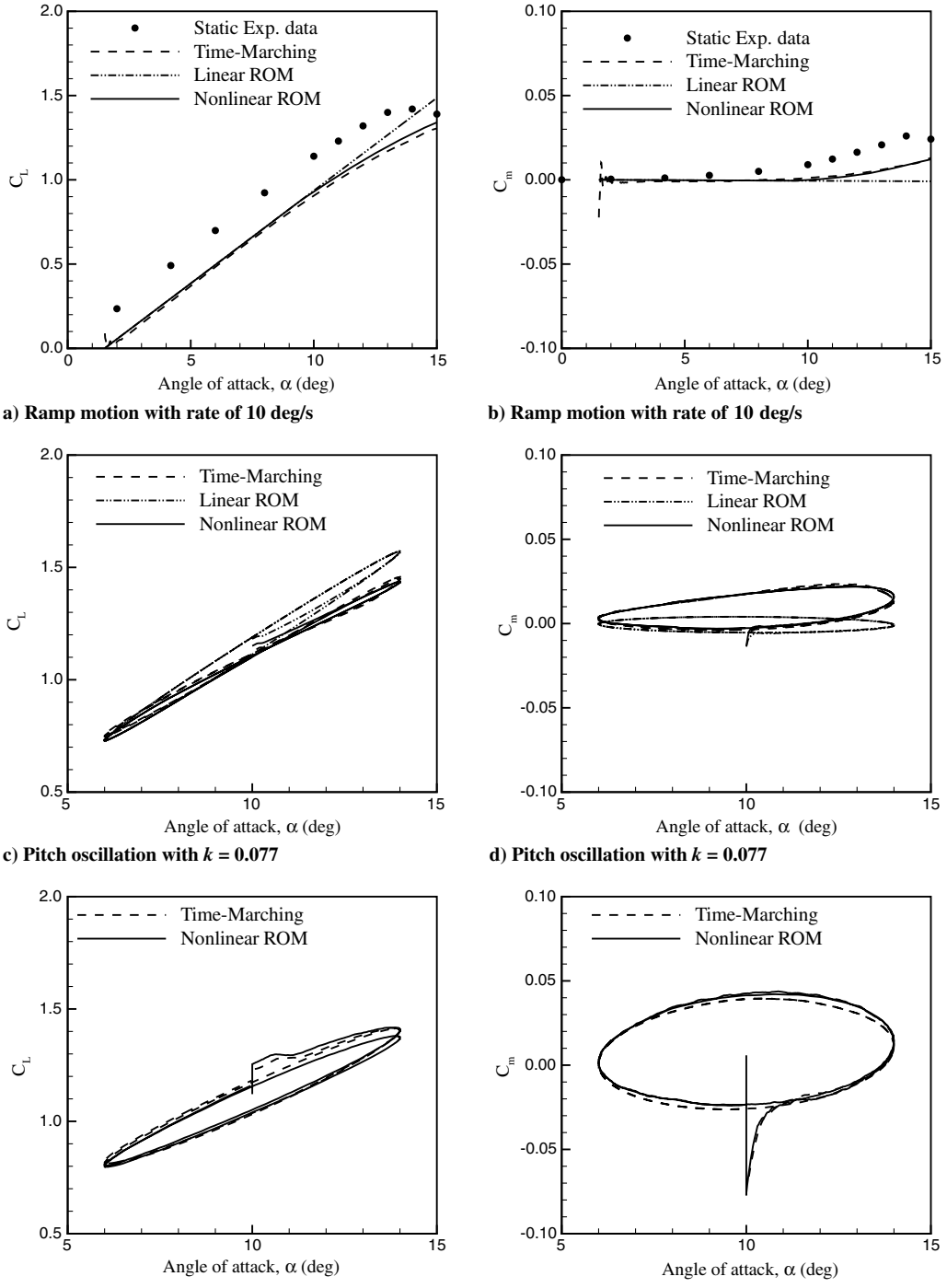

a) Ramp motion with rate of 10 deg/s

b) Ramp motion with rate of 10 deg/s

c) Pitch oscillation with $k = 0.077$

d) Pitch oscillation with $k = 0.077$

e) Pitch oscillation with $k = 0.307$

f) Pitch oscillation with $k = 0.307$

Fig. 9 Nonlinear indicial response ROM model for NACA 0012, $M_\infty = 0.3$ and $Re = 5.93 \times 10^6$.

loads can be determined even with using Euler equations, as shown by Lomax [49].

Figures 9a and 9b compare the linear and nonlinear ROM predictions for a ramp increase of angle of attack from 1.5 to 15 deg with a rate of 10 deg /s. The grid is undergoing only a translational motion, so the second terms in Eqs. (7–9) are zero. Note that the forces and moments acting on the airfoil during translation are different from the static values. The flow change is not as fast as the angle-of-attack change, and hence the ramp motion underestimates the static coefficients. The results show for low angles of attack, both linear and nonlinear ROMs have good agreement with values of the full-order simulation. For large angles of attack, the nonlinear model closely follows the time-marching solution, but the linear model is off, since the model formulation is valid in linear regimes. Figures 9c–9f show two pitch-oscillation cases with reduced frequencies of $k = 0.077$ and 0.307, with mean incidence α_0 of 10 deg and amplitude α_a of 4 deg. The figures show that the nonlinear ROM predictions agree well with full-order simulation values. In Table 2, the costs to train the ROMs, that of executing the ROMs and of running the full-order model, are compared. The airfoil computations were performed on 10 nodes, where each node has two dual-core AMD processor running at 1 GHz. The linear and nonlinear models required about 0.6 and 6.0 h of CPU time, respectively. The nonlinear model requires response calculations at different angles of attack and hence comes with more computational cost. The nonlinear ROM requires more execution time, due to the used interpolation scheme. Once the ROMs are constructed, they can be used for rapid prediction of a wide range of pitching and plunging motions.

Table 2 Computational cost comparisons: airfoil

	Training ROMs (CPU, h)	Executing ROMs (CPU, s)	Full-order model (CPU, h)
Linear ROM	0.6	——	——
Linear pitch $k = 0.077$	——	100	1.8 per cycle
Linear pitch $k = 0.307$	——	40	0.8 per cycle
Nonlinear ROM	6.0	——	——
Nonlinear ramp	——	50	0.3
Nonlinear pitch $k = 0.077$	——	210	1.8 per cycle
Nonlinear pitch $k = 0.307$	——	80	0.8 per cycle

Table 3 Computational cost comparisons: SACCON UCAV

	Training ROMs (CPU, h)	Executing ROMs (CPU, s)	Full-order model (CPU, h)
Linear ROM	0.73	——	——
Linear pitch $k = 0.157$	——	50	5 per cycle
Chirp maneuver	——	60	5
Nonlinear ROM	7.3	——	——
Nonlinear pitch $k = 0.157$	——	120	5 per cycle

B. SACCON UCAV

SACCON motion files were generated for a unit step change in angle of attack and pitch rate at a zero-degree angle of attack. These files define the rotations and displacements at discrete time instants. At each computational time step, Cobalt then interpolates motion data using cubic-splines and moves the grid. All computations started from a steady-state solution and then advanced in time using second-order accuracy with five Newton subiterations. The number of iterations were found from the motion time divided by the physical time step. The sensitivity of solutions to time step was also investigated. The corresponding lift and pitching-moment responses to a unit change in angle of attack are shown in Figs. 10a and 10b with three different nondimensional time steps ($\Delta s = 0.001$, 0.002, and 0.01). The smallest size solution is plotted only at each 100 time steps. The figures show that predictions of small and medium time steps coincide with each other and match well with the large time step

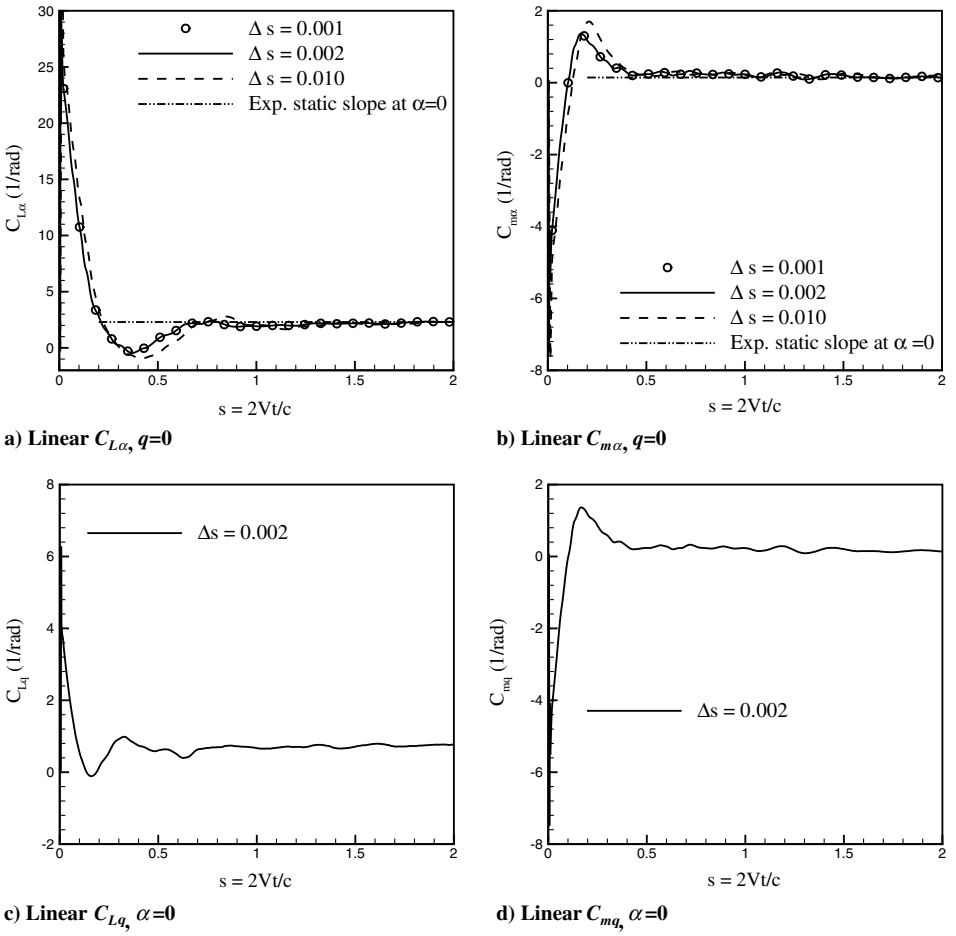

Fig. 10 Indicial function of SACCON UCAV. The lift and pitching-moment indicial functions with unit step change of angle of attack and pitch rate are shown at $M_\infty = 0.144$ and $Re = 1.61 \times 10^6$.

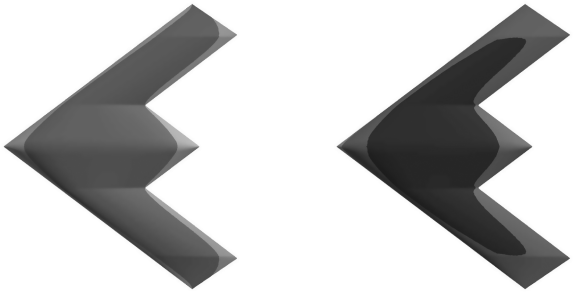

a) Steady $\alpha = 0$ **b) Step in angle of attack, $s = 0$**

Fig. 11 Flow streamline changes for a step change in angle of attack.

at initial and final time steps. Therefore, the medium time step $\Delta s = 0.002$ was used for simulation of all motions.

As shown in Fig. 10a, the lift response has a peak at $s = 0$. Likewise, the pitching-moment predicts a negative peak at this time. As the steady flow around the vehicle is disturbed by the grid motion, an acoustic wave propagates from the bottom of the vehicle upstream and then to the top of the vehicle downstream, causing a sudden increase of angle of attack and lift coefficient at this time. The flow streamlines over the upper wing surface at $s = 0$ are compared with the steady solution in Fig. 11. The figure shows a traveling wave in the flow as grid starts to move. As the response time increases, the surrounding flow around the aircraft will be dominated by the transport of vorticity shed into the wake [56]. The lift response then starts to fall and then asymptotically reaches the steady-state value. Figures 10a and 10b show that the calculated steady-state values agree well with the slope of coefficients found from static experimental data. In comparison with the airfoil case, SACCON has a much faster response time, which is mainly due to the three-dimensional mechanism of vorticity shed into the wake, which is completely different from two-dimensional airfoils, due to the lack of tip vortices [56].

Figure 10 also shows the indicial lift and pitching-moment coefficients with normalized pitch rate as a function of normalized time (s). Likewise, for the angle-of-attack step motion, the lift peaks up and the pitching moment has a negative peak at $s = 0$. The angle of attack remains zero during rotations; thus, all the effects are from the pitch rate.

The linear ROM was created using Eqs. (7) and (8) and used for prediction of a pitch oscillation and a frequency-sweep motion. The pitch-oscillation mean angle of attack is zero with an amplitude of 1 ° and frequency of 5 Hz. The calculations start from a steady solution at a zero-degree angle of attack and run only for one cycle using the medium time step. Figures 12a and 12b compare the linear ROM lift and pitching-moment predictions with time-marching simulations. The results show a well matched comparison between ROM predictions and time-marching solutions. The model also accurately predicts the initial peaks in full-order simulations at the beginning of the oscillations.

The frequency-sweep maneuver, also named a chirp, is often used to identify the aerodynamics characteristics of aircraft pitch motions [15]. The vehicle is undergoing an oscillatory movement around the reference point with an increasing frequency. The angle of attack at each time is

$$\alpha(t) = \alpha_0 + \alpha_A \sin(\omega t^2) \tag{15}$$

A chirp maneuver with 2 deg amplitude, zero mean angle of attack, and 2π rad/s frequency was simulated using Cobalt. The simulation runs up to 2 s of physical time. Again, the motion calculations start from the steady solution at a zero-degree angle of

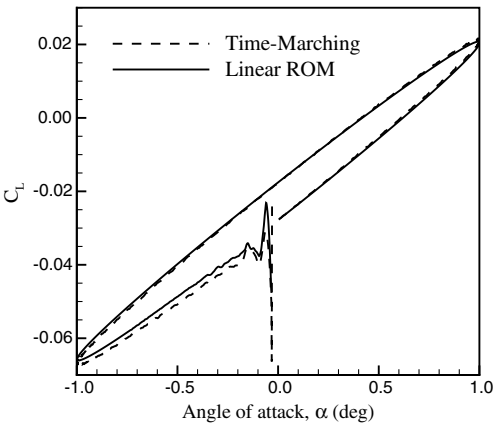

a) Pitch oscillation with $k = 0.157$

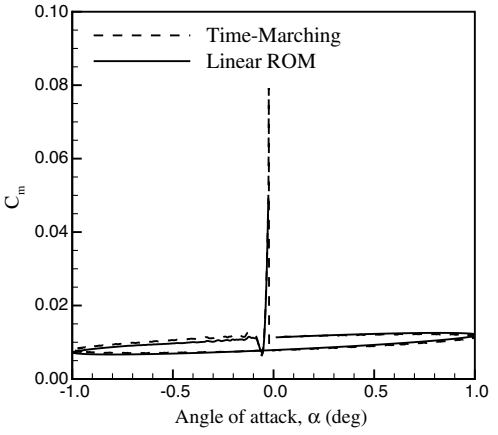

b) Pitch oscillation with $k = 0.157$

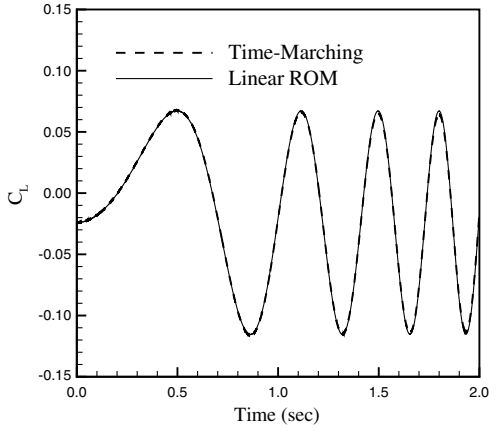

a) Chirp maneuver

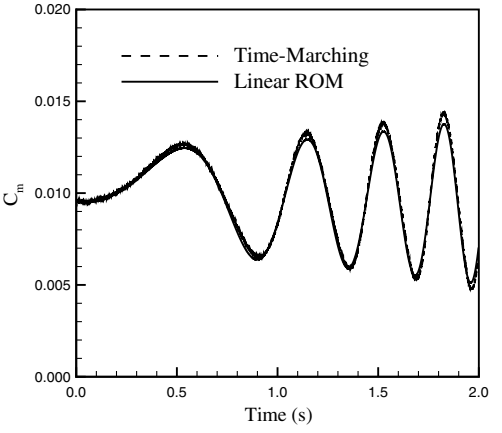

b) Chirp maneuver

Fig. 12 Linear ROM and time-marching solutions for pitch oscillating and chirp motions of SACCON at $M_\infty = 0.144$ and $Re = 1.61 \times 10^6$.

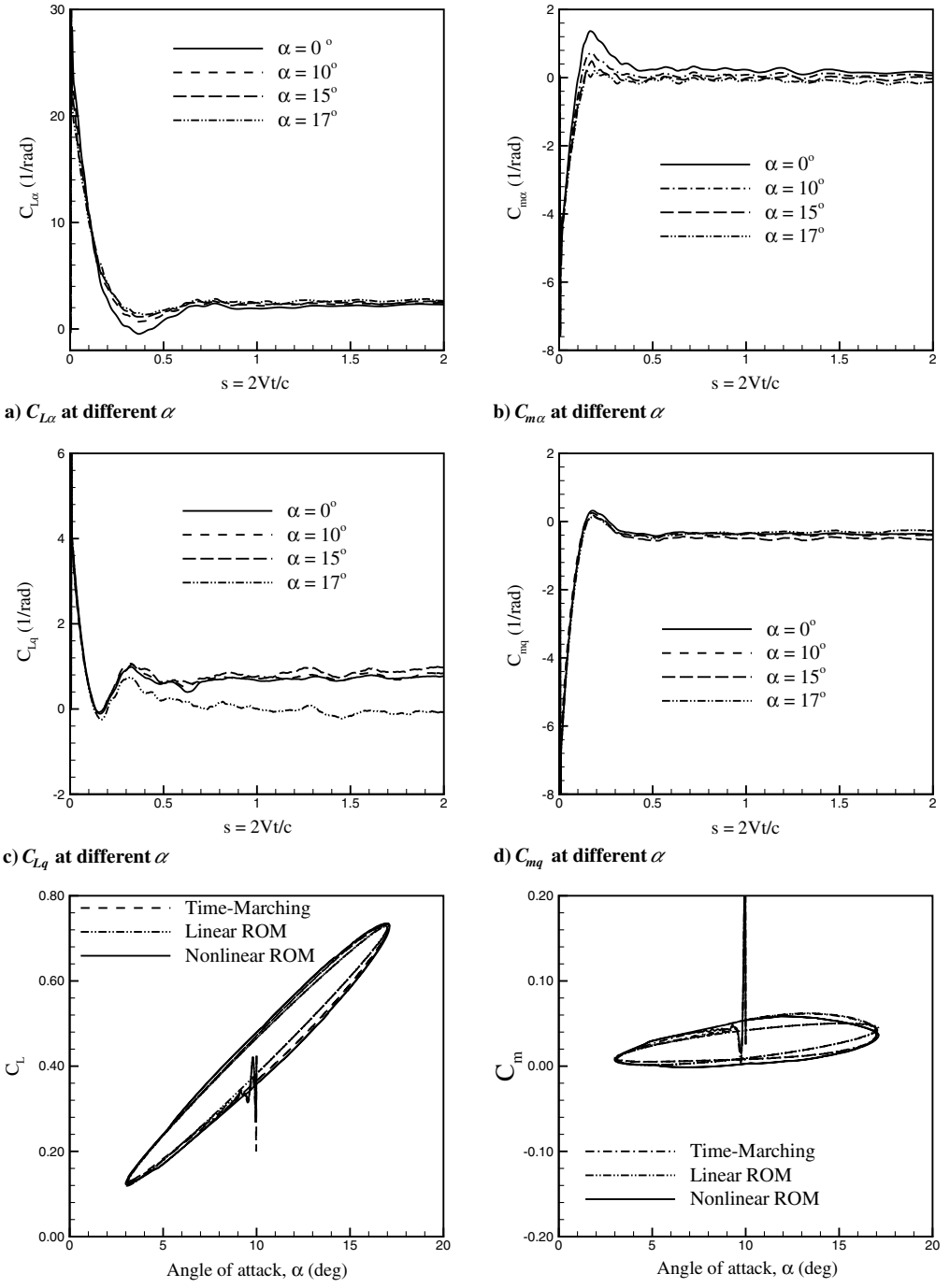

a) $C_{L\alpha}$ **at different** α **b)** $C_{m\alpha}$ **at different** α

c) C_{Lq} **at different** α **d)** C_{mq} **at different** α

e) Pitch oscillation with $k = 0.157$ **f) Pitch oscillation with** $k = 0.157$

Fig. 13 Nonlinear responses of SACCON UCAV. Flow conditions are $M_\infty = 0.144$ **and** $Re = 1.61 \times 10^6$**.**

attack with the medium time step. The lift and pitching-moment responses are shown in Figs. 12c and 12d and compared with the ROM predictions. An excellent match was found between simulations and predictions.

The indicial functions vary with angle of attack and Fig. 13 shows the aircraft responses at different angles of attack. The initial values are invariant with angle of attack, but the transient trend and steady-state values change, depending on the angle of attack. These function along with an interpolation scheme are used to determine the terms in Eqs. (9) at each time step. Figure 13 also shows a pitch-oscillation case with a frequency of 5 Hz, with mean incidence α_0 of 10 deg and amplitude α_a of 7 deg. The figures show that the nonlinear ROM predictions agree well with full-order simulation values, while linear ROM cannot predict the nonlinearities. Table 3 compares the costs to train the ROMs, of executing the ROMs, and of running the full-order model. The linear and nonlinear models required about 0.7 and 7.0 h of CPU time, respectively. The ROM/full-order cost ratio for SACCON is smaller than those obtained for an airfoil, since SACCON has a much faster response time. Again, once the ROMs are constructed, they can be used for rapid prediction of a wide range of pitching and plunging motions.

VII. Conclusions

This work investigates the use of a reduced-order model (ROM) for unsteady and nonlinear aerodynamic loads modeling. The ROM considered is an indicial theory based on the convolution of a step function with the derivative of the input signal. The aircraft step functions can only be determined by CFD calculations and grid motion tools. The longitudinal aerodynamic forces and moments are only considered; thus, the aircraft responses corresponding to a step change in angle of attack and pitch rate are found. For the pitch rate,

the grid moves such that the angle of attack remains unchanged. For the linear ROM, the responses at a zero-degree angle of attack are used. For modeling the nonlinear forces and moments, the indicial functions at different angles of attack are also found.

The test cases used were the NACA 0012 airfoil and the SACCON UCAV. All CFD calculations were performed using the solution of URANS equations and the SARC turbulence model. Validations were made against available experimental data. A good agreement was found in both cases. A time-step sensitivity study also was performed for SACCON time-dependent calculations.

The results show that indicial functions have a peak at initial time steps. This is related to a traveling acoustic wave formed by the flow disturbance. At higher Mach numbers, the peak values are diminished due to compressibility. The responses reach a steady-state value at the final time steps. The analytical solutions are available only for airfoils at the initial and final points, but the CFD responses compare favorably with the analytical solutions.

The ROMs are tested by comparison of the model output with time-accurate CFD simulations for several maneuvers. At low angles of attack, the linear ROM results in an excellent match with time-marching solutions. At higher angles of attack, the nonlinearities are captured with a nonlinear ROM, for both slow and fast pitching motions. The ROMs used also predicts the initial peaks at time-marching simulations.

Future work will extend this study to include high-speed and lateral aerodynamics modeling. This includes the response functions with respect to sideslip angle, roll, and yaw rates. Then the ROMS will be tested for some realistic 6-DOF aircraft maneuvers and will be compared against other models. The possibility of a faster generation of aerodynamic responses using Euler grids and data fusion will also be considered.

Acknowledgments

Mehdi Ghoreyshi and Adam Jirásek were supported by the National Research Council and U.S. Air Force Office of Scientific Research. Their financial support is gratefully acknowledged. Computer time was provided by the U.S. Department of Defense Arctic Region Supercomputing Center (ARSC). The authors appreciate the support provided by the Modeling and Simulation Research Center at the U.S. Air Force Academy. SACCON (Stability and Control Configuration) geometry and wind-tunnel data were provided by NATO RTO Task Group AVT-161 on Assessment of Stability and Control Prediction Methods for NATO Air and Sea Vehicles.

References

[1] Mason, W. H., Knill, D. L., Giunta, A. A., Grossman, B., Watson, L. T., and Haftka, R. T., "Getting the Full Benefits of CFD in Conceptual Design," AIAA Paper 98-2513, June 1998.

[2] Raymer, D. P., *Aircraft Design: A Conceptual Approach*, 4th ed., AIAA Education Series, AIAA, Reston, VA, 2006.

[3] Roskam, J., *Airplane Design*, Roskam Aviation and Engineering Corp., Ottawa, KS, 1990.

[4] Arndt, M., Brandt, S., and Bergeron, K., "Conceptual Design and Computational Investigation of Stabilator Mounted Coplanar with Wing," AIAA Paper 2010-1428, Jan. 2010.

[5] Tobak, M., and Schiff, L. B., "Generalized Formulation of Nonlinear Pitch-Yaw-Roll Coupling: Part 1: Nonaxisymmetric Bodies," *AIAA Journal*, Vol. 13, No. 3, 1975, pp. 323–326. doi:10.2514/3.49698

[6] Tobak, M., and Schiff, L. B., "Generalized Formulation of Nonlinear Pitch-Yaw-Roll Coupling: Part 2: Nonlinear Coning-Rate Dependence," *AIAA Journal*, Vol. 13, No 3, 1975, pp. 327–332. doi:10.2514/3.49699

[7] Abramov, N. B., Goman, M. G., Greenwell, D. I., and Khrabrov, A. N., "Two-Step Linear Regression Methods for Identification of High Incidence Unsteady Aerodynamic Model," AIAA Paper 2001-4080, Aug. 2001.

[8] Lisandrin, P., Carpentieri, G., and van Tooren, M., "Investigation over CFD-Based Models for the Identification of Nonlinear Unsteady Aerodynamics Responses," *AIAA Journal*, Vol. 44, No. 9, 2006, pp. 2043–2050. doi:10.2514/1.18726

[9] McDaniel, D. R., Cummings, R. M., Bergeron, K., Morton, S. A., and Dean, J. P., "Comparisons of CFD Solutions of Static and Maneuvering Fighter Aircraft with Flight Test Data," *Journal of Aerospace Engineering*, Vol. 223, No. 4, 2009, pp. 323–340. doi:10.1243/09544100JAERO411

[10] Greenwell, D. I., "A Review of Unsteady Aerodynamic Modelling for Flight Dynamics of Manoeuvrable Aircraft," AIAA Paper 2004-5276, Aug. 2004.

[11] Ghoreyshi, M., Badcock, K. J., Woodgate, M. A., "Accelerating the Numerical Generation of Aerodynamic Models for Flight Simulation," *Journal of Aircraft*, Vol. 46, No. 3, 2009, pp. 972–980. doi:10.2514/1.39626

[12] Ghoreyshi, M., Da Ronch, A., Badcock, K. J., Dees, A., Berard, A., and Rizzi, A., "Aerodynamic Modelling for Flight Dynamics Analysis of Conceptual Aircraft Designs," AIAA Paper 2009-4121, June 2009.

[13] Ghoreyshi, M., Badcock, K. J., Da Ronch, A., Swift, A., Marques, S., and Ames, N., "Framework for Establishing the Limits of Tabular Aerodynamic Models for Flight Dynamics Analysis," *Journal of Aircraft*, Vol. 48, No. 1, 2011, pp. 42–55. doi:10.2514/1.C001003

[14] Ghoreyshi, M., Vallespin, D., Da Ronch, A., Badcock, K. J., Vos, J., and Hitzel, S., "Simulation of Aircraft Manoeuvres Based On Computational Fluid Dynamics," AIAA Paper 2010-8239, Aug. 2010.

[15] Tischler, M. B., and Remple, R. K., *Aircraft and Rotorcraft System Identification: Engineering Methods with Flight Test Examples*, AIAA Education Series, AIAA, Reston, VA, 2006.

[16] Lucia, D. J., Beran, P. S., and Silva, W. A., "Reduced-Order Modeling: New Approaches For Computational Physics," *Progress in Aerospace Sciences*, Vol. 40, 2004, pp. 51–117. doi:10.1016/j.paerosci.2003.12.001

[17] Jategaonkar, R. V., *Flight Vehicle System Identification*, AIAA Educational Series, Vol. 216, AIAA, Reston, VA, 2006.

[18] Ballhaus, W. F., and Goorjian, P. M., "Computation of Unsteady Transonic Flows by Indicial Methods," *AIAA Journal*, Vol. 16, No. 2, 1978, pp. 117–124. doi:10.2514/3.60868

[19] Tobak, M., Chapman, G. T., and Schiff, L. B., "Mathematical Modeling of the Aerodynamic Characteristics in Flight Dynamics," NASA TM-85880, 1984.

[20] Tobak, M., and Chapman, G. T.,"Nonlinear Problems in Flight Dynamics Involving Aaerodynamic Bifurcations," NASA TM-86706, 1985.

[21] Hall, K. C., Thomas, J. P., and Dowell, E. H., "Reduced-order Modelling of Unsteady Small-Disturbance Using a Frequency-Domain Proper Orthogonal Decomposition Technique," AIAA Paper 1999-655, Jan. 1999.

[22] Gaitonde, A., and Jones, D. P., "Reduced Order State-Space Models from the Pulse Responses of a Linearized CFD Scheme," *International Journal for Numerical Methods in Fluids*, Vol. 42, No. 6, 2003, pp. 581–606. doi:10.1002/fld.527

[23] Silva, W. A., and Bartels, R. E., "Development of Reduced-Order Models for Aeroelastic Analysis and Flutter Prediction Using the CFL3Dv6.0 Code," *Journal of Fluids and Structures*, Vol. 19, No. 6, 2004, pp. 729–745. doi:10.1016/j.jfluidstructs.2004.03.004

[24] Jirásek, A., Jeans, T. L., Martenson, M., Cummings, R. M., and Bergeron, K., "Improved Methodologies for Maneuver Design of Aircraft Stability and Control Simulations," AIAA Paper 2010-515, Jan. 2010.

[25] Goman, M. G., and Khrabov, A. N.,"State-Space Representation of Aerodynamic Characteristics of An Aircraft at High Angles of Attack," AIAA Paper 92-4651, Aug. 1992.

[26] Jirásek, A., and Cummings, R. M., "Application of Volterra Functions to X-31 Aircraft Model Motion," AIAA Paper 2009-3629, June 2009.

[27] Görtz, S., McDaniel, D. R., and Morton, S. A., "Towards an Efficient Aircraft Stability and Control Analysis Capability Using High-Fidelity CFD," AIAA Paper 2007-1053, Jan. 2007.

[28] Jirásek, A., and Cummings, R. M., "Reduced Order Modelling of X-31 Wind Tunnel Model Aerodynamic Loads," AIAA Paper 2010-4693, June–July 2010.

[29] Singh, R., and Baeder, J. D., "Direct Calculation of Three-Dimensional Indicial Lift Response Using Computational Fluid Dynamics," *Journal of Aircraft*, Vol. 34, No. 4, 1997, pp. 465–471. doi:10.2514/2.2214

[30] Korenberg, M. J., and Hunter, I. W., "The Identification of Nonlinear Biological Systems: Volterra Kernel Approaches," *Annals of Biomedical Engineering*, Vol. 24, 1996, pp. 250–268.

doi:10.1007/BF02667354
[31] Volterra, V., *Theory of Functionals*, Blackie, London, 1930.
[32] Wiener, N., *Nonlinear Problems in Random Theory*, MIT Press, Cambridge, MA, 1958.
[33] Barrett, J. F., "The Use of Functionals in the Analysis of Nonlinear Physical Systems," *Journal of Electronics and Control*, Vol. 15, 1963, pp. 567–615.
doi:10.1080/00207216308937611
[34] Kalman, R. E., "Pattern Recognition Properties of Multilinear Response Functions," *Control and Cybernetics*, Pt. I, Vol. 9, 1980, pp. 5–31.
[35] Stark, L., *Neurological Control System*, Studies in Bioengineering, Plenum, New York, 1968.
[36] Weiner, D. D., and Spina, J. F., *Sinusoidal Analysis and Modeling of Weakly Nonlinear Circuits*, Van Nostrand Reinhold, New York, 1980.
[37] Hunter, I. W., and Korenberg, M. J., "The Identification of Nonlinear Biological Systems: Wiener and Hammerstein Cascade Models," *Biological Cybernetics*, Vol. 55, 1986, pp. 135–144
[38] Korenberg, M. J., "A Fast Orthogonal Search Method For Biological Time-Series Analysis and System Identification," *IEEE International Conference on Systems, Man and Cybernetics*, Vol. 2, IEEE Press, Piscataway, NJ, 1989, pp. 459–465.
doi:10.1109/ICSMC.1989.71337
[39] Korenberg, M. J., "A Robust Orthogonal For System Identification and Time-Series Analysis," *Biological Cybernetics*, Vol. 60, 1989, pp. 267–276.
doi:10.1007/BF00204124
[40] Silva, W. A., "Identification of Nonlinear Aeroelastic Systems Based on the Volterra Theory: Progress and Opportunities," *Nonlinear Dynamics*, Vol. 39, Nos. 1–2, 2005, pp. 25–62.
doi:10.1007/s11071-005-1907-z
[41] Schetzen, M., "Measurement of the Kernels of a Non-Linear System of Finite Order," *International Journal of Control*, Vol. 1, No. 3, 1965, pp. 251–263.
doi:10.1080/00207176508905477
[42] Schetzen, M., *The Volterra and Weiner Theories of Nonlinear Systems*, Wiley, New York, 1980.
[43] Dasgupta, D., and Michalewicz, Z., *Evolutionary Algorithms in Engineering Applications*, Springer–Verlag, Berlin, 1997.
[44] Leishman, L. G., "Indicial Lift Approximations for Two-Dimensional Subsonic Flow as Obtained from Oscillatory Measurements," *Journal of Aircraft*, Vol. 30, No. 3, 1993, pp. 340–351.
doi:10.2514/3.46340
[45] Duffy, D. G., *Advanced Engineering Mathematics With MATLAB*, 2nd ed., Chapman and Hall/CRC, Boca Raton, FL, 2003.
[46] Reisenthel, P. H., "Development of a Nonlinear Indicial Model Using Response Functions Generated by a Neural Network," AIAA Paper 97-0337, Jan. 1997.
[47] Reisenthel, P. H., and Bettencourt, M. T., "Data-Based Aerodynamic Modeling Using Nonlinear Indicial Theory," AIAA Paper 99-0763, Jan. 1999.
[48] Raveh, D. E., "Reduced-Order Models for Nonlinear Unsteady Aerodynamics," *AIAA Journal*, Vol. 39, No. 8, 2001, pp. 1417–1429.
doi:10.2514/2.1473
[49] Lomax, H., "Indicial Aerodynamics," *Manual of Aeroelasticity*, AGARD, Part 2, Neuilly-sur-Seine, France, Chap. 6, 1960.
[50] Wagner, H., "Über die Entstehung des Dynamischen Auftriebes von Tragflügeln," *Zeitschrift für Angewandte Mathematik und Mechanik*, Vol. 5, No. 1, 1925, pp. 17–35.
doi:10.1002/zamm.19250050103
[51] Leishman, J. G., and Nguyen, K. Q.,"State-Space Representation of Unsteady Airfoil Behaviour," *AIAA Journal*, Vol. 28, No. 5, 1990, pp. 836–844.
doi:10.2514/3.25127
[52] Bisplinghoff, R. L., Ashley, H., and Halfman, R. L., *Aeroelasticity*, Dover, Mineola, NY, 1996.
[53] Mazelsky, B., "On the Noncirculatory Flow About a Two-Dimensional Airfoil at Subsonic Speeds," *Journal of the Aeronautical Sciences*, Vol. 19, No. 12, 1952, pp. 848–849.
[54] Queijo, M. J., Wells, W. R., and Keskar, D. A., "Approximate Indicial Lift Function for Tapered, Swept Wings in Incompressible Flow," NASA TP-1241, 1978.
[55] Yee, K., Hong, S., and Lee, D., "Numerical Investigation on the Directionally of Nonlinear Indicial Responses," *Journal of Mechanical Science and Technology*, Vol. 21, 2007, pp. 1293–1305.
doi:10.1007/BF03179046
[56] Manglano-Villamarin, C. E., and Shaw, S. T., "Three-Dimensional Indicial Response of Finite Aspect Ratio Yawed Wings," *The Aeronautical Journal*, Vol. 111, No. 1120, 2007, pp. 359–371
[57] Wurtzler, K. E., and Morton, S. A.,"Accurate Drag Prediction Using Cobalt," AIAA Paper 2004-0395, Jan. 2004.
[58] Gottlieb, J. J., and Groth, C. P. T., "Assessment of Riemann Solvers for Unsteady One-Dimensional Inviscid Flows of Perfect Gasses," *Journal of Computational Physics*, Vol. 78, No. 2, 1988, pp. 437–458.
doi:10.1016/0021-9991(88)90059-9
[59] Tomaro, R. F., Strang, W. Z., and Sankar, L. N.,"An Implicit Algorithm For Solving Time Dependent Flows on Unstructured Grids," AIAA Paper 97-0333, Jan. 1997.
[60] Forsythe, J. R., Hoffmann, K. A., Cummings, R. M., and Squires, K. D., "Detached-Eddy Simulation with Compressibility Corrections Applied to a Supersonic Axisymmetric Base," *Journal of Fluids Engineering*, Vol. 124, No. 4, 2002, pp. 911–923.
doi:10.1115/1.1517572
[61] Forsythe, J. R., and Woodson, S. H.,"Unsteady Computations of Abrupt Wing Stall Using Detached-Eddy Simulations," *Journal of Aircraft*, Vol. 42, No. 3, 2005, pp. 606–616.
doi:10.2514/1.2934
[62] Morton, S. A., Forsythe, J. R., Mitchell, A. M., and Hajek, D., "Detached-Eddy Simulations and Reynolds-Averaged Navier–Stokes Simulations of Delta Wing Vortical Flowfields," *Journal of Fluids Engineering*, Vol. 124, No. 4, 2002, pp. 924–932.
doi:10.1115/1.1517570
[63] Forsythe, R., Squires, K. D., Wurtzler, K. E., and Spalart, P. R., "Detached-Eddy Simulation of Fighter Aircraft at High Alpha," *Journal of Aircraft*, Vol. 41, No. 2, 2004, pp. 193–200.
doi:10.2514/1.2111
[64] Jeans, T., McDaniel, D., Cummings, R. M., and Mason, W., "Aerodynamic Analysis of a Generic Fighter Using Delayed Detached-Eddy Simulations," *Journal of Aircraft*, Vol. 46, No. 4, 2009, pp. 1326–1339.
doi:10.2514/1.40955
[65] Ladson, C. L., "Effects of Independent Variation of Mach and Reynolds Number on the Low-Speed Aerodynamic Characteristics of NACA 0012 Airfoil Section," NASA TM-4074, 1988.
[66] Landon, R. H., "NACA 0012: Oscillating and Transient Pitching," AGARD, Rept. R-702, Neuilly-sur-Seine, France, 1982.
[67] Cummings, R. M., Morton, S. A., and McDaniel, D. R.,"Experiences in Accurately Predicting Time-Dependent Flows," *Progress in Aerospace Sciences*, Vol. 44, 2008, pp. 241–257.
doi:10.1016/j.paerosci.2008.01.001
[68] Cummings, R. M., and Schütte, A., "An Integrated Computational/Experimental Approach to UCAV Stability and Control Estimation: Overview of NATO RTO AVT-161," AIAA Paper 2010-4392, June–July 2010.
[69] Löser, T., Vicroy, D., and Schütte, A., "SACCON Static Wind Tunnel Tests at DNW-NWB and $14' \times 22'$ NASA LaRC.," AIAA Paper 2010-4393, June–July 2010.
[70] Schütte, A., Hummel, D., and Hitzel, S. M. "Numerical and Experimental Analyses of the Vortical Flow Around the SACCON Configuration," AIAA Paper 2010-4690, June–July 2010.
[71] Tyssel, L., "Hybrid Grid Generation for complex 3D Geometries," *Proceedings of the 7th International Conference on Numerical Grid Generation in Computational Field Simulation*, 2000, pp. 337–346.
[72] Tyssel, L., "The TRITET Grid Generation System," *Proceedings of the 10th International Conference on Numerical Grid Generation in Computational Field Simulations*, International Society of Grid Generation, Crete, Greece, 2000.
[73] Jirásek, and Cummings, R. M., "SACCON Static and Dynamic Motion Flow Physics Simulations Using COBALT," AIAA Paper 2011-3965, June 2011.

F. Ladeinde
Associate Editor